An Experimental 225 GHz Pulsed Coherent Radar

Robert W. McMillan, *Senior Member, IEEE*, C. Ward Trussell, Jr., Ronald A. Bohlander, J. Clark Butterworth, and Ronald E. Forsythe

Abstract—**An experimental coherent pulsed radar operating at 225 GHz is described. This system uses a pulsed, phase-locked extended interaction oscillator transmitter and an $f/4$ (frequency divided by 4) subharmonic mixer pumped by a phase-locked Gunn oscillator as the receiver. A quasi-optical circular polarization duplexer combines transmitter and receiver signals into the same antenna. Results obtained with this system include the detection of targets out to ranges of 3.5 km and observation of Doppler spectra of trucks and tracked vehicles, including contributions from both body and tracks.**

I. Introduction

SINCE the very early days of radar, system designers have looked toward the higher microwave and millimeter-wave (MMW) frequencies for the purposes of improving resolution and/or reducing antenna and other component sizes. During the last few years, the significant improvements made in MMW componentry have provided the means for moving higher in frequency, up to bands where the atmosphere, rather than component availability, imposes severe limitations on radar performance [1]. Of the atmospheric transmission bands available for use in ground-based radar applications, the region broadly centered near 230 GHz is perhaps the highest frequency band that is of practical use. A radar operating in this band was recently described by McIntosh *et al.* [2], [3]. This radar has been used to obtain some excellent measurements on backscattering from various surfaces and materials [4]. There is also a narrow atmospheric window centered at 340 GHz, but attenuation caused by water vapor in this window may exceed 10 dB/km under conditions of high humidity. This latter window has been proposed for use in submillimeter-wave imaging systems, however [5].

This paper describes a 225 GHz coherent radar system with the following subsystems:

1) a pulsed, phase-locked extended interaction oscillator (EIO) transmitter;
2) an all-solid-state receiver comprising a Gunn local oscillator (LO) operating at 56 GHz with an $f/4$ (frequency divided by 4) subharmonic mixer;
3) a quasi-optical circular polarization duplexer which uses an antireflection-coated sapphire quarter-wave plate and a polarizing metal wire grid array to separate the transmit and receive signals;
4) a 15 cm plastic lens antenna.

The Gunn LO is phase locked to a crystal reference oscillator, and the transmitter is in turn locked to the Gunn during its output pulse. Significant achievements of this radar include the observation of targets out to ranges of 3.5 km and the measurement of Doppler spectra due to moving targets such as trucks and tracked vehicles (with a separate contribution observable from the treads).

Manuscript received April 17, 1990; revised August 21, 1990. This work was supported by the U.S. Army CECOM Center for Night Vision and Electro-Optics under Contract DAAK70-79-C-0108.

R. W. McMillan and R. A. Bohlander are with the Georgia Institute of Technology, Georgia Tech Research Institute, Atlanta, GA 30332.

C. W. Trussell, Jr., is with the U.S. Army Communications—Electronic Command, Center for Night Vision and Electro-Optics, Ft. Belvoir, VA 22060.

J. C. Butterworth was with the Georgia Institute of Technology, Georgia Tech Research Institute, Atlanta, GA. He is now with Pulse Technology, Inc., Kennesaw, GA 30144.

R. E. Forsythe is with Forsythe Technologies, Atlanta, GA.

IEEE Log Number 9041464.

II. General Description

Fig. 1 is a simplified block diagram of the radar. The 56 GHz Gunn LO is phase locked to the 98 MHz crystal reference oscillator. The Gunn output is split and half is used to phase-lock the EIO while the other half serves as LO for the $f/4$ subharmonic receiver mixer. The EIO phase-locking control voltage is fed back to the tube body, which is isolated from other tube electrodes but is connected to the output waveguide, so that an isolating flange is required as shown. The linearly polarized EIO output passes through a wire grid beam splitter with its grid wires oriented perpendicular to the plane of polarization of the radiation. The output is then focused by the conically scanning (conscan) lens and collimated by the antenna lens. The conscan tracking function was not implemented because of budget limitations. The signal then passes through the quarter-wave plate, from whence it emerges with circular polarization. The radiation is steered to the target by a gimbaled mirror. Upon reflection from a target, the radiation has its sense of circular polarization reversed, assuming an odd-bounce target, and on passing again through the quarter-wave plate, emerges with linear polarization orthogonal to that entering from the EIO. Since the grid wires are now parallel to the plane of polarization, the radiation is reflected into the receiver horn, where it mixes with the fourth harmonic of the LO to give a 781 MHz intermediate frequency (IF). This IF is amplified and compared with a harmonic of the crystal reference oscillator in in-phase and quadrature modes to give pulsed outputs whose frequency is proportional to the radial velocity of the target. Fig. 2 is a photograph of the radar, which is shown mounted on a 1.2×1.2 m aluminum plate which is in turn mounted on a pedestal. A television camera, bore-

0018-9480/91/0300-0555$01.00 ©1991 IEEE

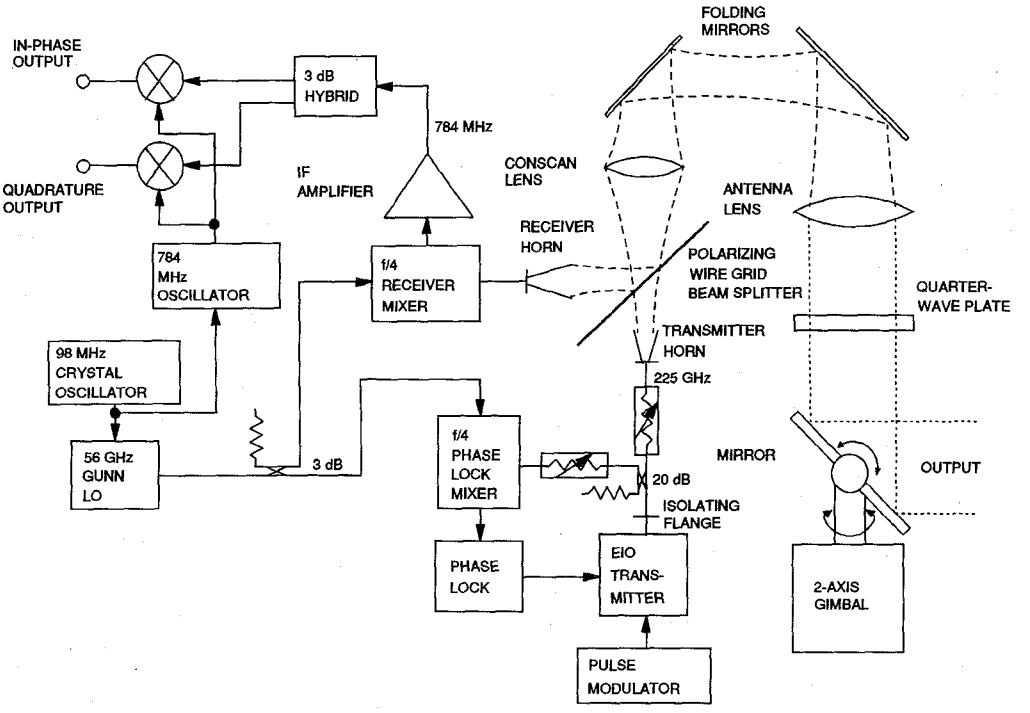

Fig. 1. Simplified block diagram of the radar showing the relationships of the subsystems and derivation of the transmitter, receiver, and IF signals.

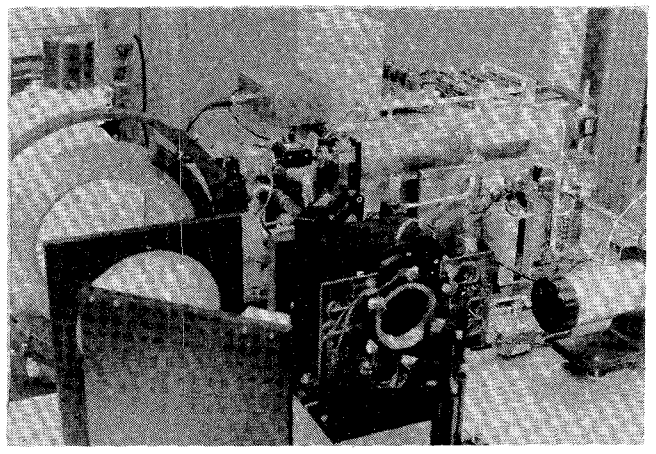

Fig. 2. Photograph of the radar. The quarter-wave plate, primary lens, and gimbal are on the left. The conscan lens is in the center, and the EIO can just be seen slightly left of center. The EIO modulator is in the rear, and the receiver LO is in front of it. The receiver and phase-lock mixers are hidden by other components.

sighted with the radar steering mirror, is used to provide visual images of the target scene. Each of the major radar subsystems is discussed separately in the sections that follow.

III. Transmitter

The EIO is a beam-power electron tube that depends for its operation on the interaction of a collimated electron beam with a metal periodic structure [6], [7]. The beam passes through the structure and is modulated by it in a manner similar to the process occurring in traveling-wave and backward-wave oscillator tubes. EIO's are available in pulsed and CW versions at frequencies in the range 35–260 GHz.

TABLE I
Specifications of Radar Transmitter

Parameter	Value
Frequency	225.445 GHz
Power Output	60 W Peak
Transmitter Path Losses	4.8 dB
Pulse Repetition Frequency	5–20 kHz
Pulse Width	50–500 ns
Transmitter Tube Type	Varian VKY-2429R EIO
Maximum Duty Factor	0.005

The specifications of the radar transmitter are given in Table I. Note that combinations of pulse repetition frequencies (PRF's) and pulse widths which exceed the tube duty factor are not allowed. The EIO output of 60 W is reduced to about 20 W by the isolating flange section, the directional coupler, and an attenuator placed in this path to prevent receiver damage. This loss could be reduced by perhaps 3 dB by more careful design and elimination of the attenuator, which was always adjusted for minimum attenuation after initial system tests showed that the receiver would not be damaged by stray radiation from the full EIO output.

The EIO is turned on by applying a negative voltage to the cathode by means of a modulator; the body of the tube runs nominally at ground potential. The transmitter modulator is perhaps the most important subsystem with regard to coherent operation of the radar, since the flatness and lack of transients on the modulator pulse determine the quality of the spectral output of the EIO. If this spectrum is not good enough, the phase lock will not be able to control the output phase of the tube, and coherent operation will not be possible. Specifically, the modulator pulse voltage (approximately 8 kV) must be flat to within about ± 20 V, which is the output range of the phase-lock driver; otherwise the phase-

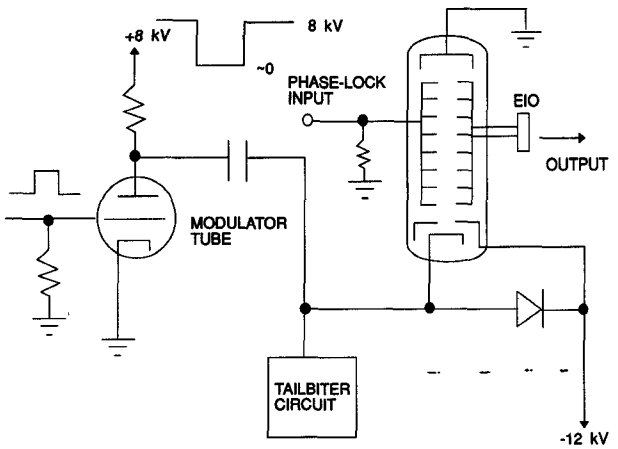

Fig. 3. Simplified schematic of the EIO modulator. The output of this circuit changes little during the radar pulse because the modulator tube is saturated.

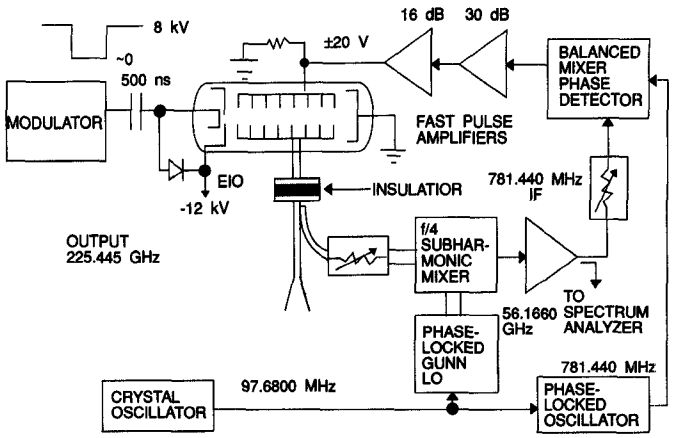

Fig. 4. Block diagram of the EIO phase lock circuitry.

lock driver will saturate and the EIO will free run until the pulse settles to within normal limits. Fig. 3 is a simplified schematic diagram of the modulator, which is seen to be very straightforward in concept. Flatness of the modulator pulse is realized by simply saturating the EIO driver so that its plate voltage is essentially constant. This pulse is coupled to the EIO cathode by a capacitor. The size of this capacitor determines the amount of droop on the cathode pulse.

A problem with this type of modulator is that it does not recover very rapidly between pulses. The EIO interelectrode capacitances are charged rapidly through the low modulator tube impedance when the tube is turned on, but must discharge slowly through the modulator plate load after the tube turns off. A new pulse cannot be initiated until this discharge is essentially complete. This problem is solved by the use of a "tailbiter" circuit, which is simply another tube which turns on to discharge the interelectrode capacitances at the end of the pulse.

As expected, the phase error is greatest where the pulse is not flat, but after the first 100 ns of the pulse duration, the modulator flatness is within the ± 20 V output range of the phase lock. The tuning coefficient of the EIO is about 300 kHz/V, so that the ± 20 V output capability of the phase lock will tune the tube over a range of ± 6 MHz; the maximum electronic tuning range of the tube is 315 MHz. These issues are addressed in more detail in Section IV.

IV. Phase-Locking the Pulsed Extended Interaction Oscillator

The EIO is phase locked using the circuitry shown in block diagram form in Fig. 4. Part of the EIO output is picked off by the 20 dB directional coupler and fed into the $f/4$ subharmonic mixer, where it is compared in phase with the fourth harmonic of the phase-locked Gunn oscillator. This signal is then a pulse at the phase-lock IF of duration equal to the EIO output pulse length. This pulse is amplified by the IF amplifiers and compared in phase with the phase-lock reference oscillator using a phase detector, which gives an output proportional to the sine of the phase angle error and equal in duration to the EIO pulse. This signal is amplified by fast pulse power amplifiers and applied to the body of the EIO, where it serves to correct the voltage between cathode and body in such a way that the output phase of the EIO has a fixed relationship to the phase reference. The EIO frequency is thus locked to the reference, to a degree that will become apparent later in this section.

The phase detector shown in Fig. 4 has an output proportional to the sine of the phase error angle. There is also a time delay, d, through the phase-locking circuitry that must be considered, an initial frequency offset corrresponding to a voltage, V_{os}, on the EIO body, and a varying frequency error caused by droop of slope b on the modulator pulse. This droop is assumed linear with time because it is caused by the charging of the modulator coupling capacitor through the parallel combination of the modulator tube plate load and the EIO impedance. Also, the balanced mixer phase detector used in this system has an output proportional to the sine of the phase difference between reference and intermediate frequency. Considering these contributions, the change in output frequency of the EIO is given by

$$f(t+d) = k_d k_a k_0 [(V_{\max} \sin \phi(t) + V_{os} + b(t+d)] \quad (1)$$

where $\phi(t)$ is phase difference at time t, k_d is the phase detector sensitivity in rad/V, k_a is the gain of the amplifiers following the phase detector, k_0 is the tuning coefficient of the oscillator in MHz/V, and $V_{\max}$ is the maximum voltage available from the driver amplifier which can be applied to the frequency control electrode on the oscillator. Combining the gain coefficients into k_e, translating the time axis by $-d$, and noting that frequency is the time derivative of phase gives

$$\frac{d\phi}{dt} = k_e [V_{\max} \sin \phi(t-d) + V_{os} + bt]. \quad (2)$$

Equation (1) is solved by an iterative numerical process in which various initial conditions are assumed and the system is allowed to determine the subsequent phase behavior as time increases in small increments Δt. The phase at time $(n+1)\Delta t$ is given by

$$\phi(n+1) = \phi(n) + \frac{d\phi(n)}{dt} \Delta t. \quad (3)$$

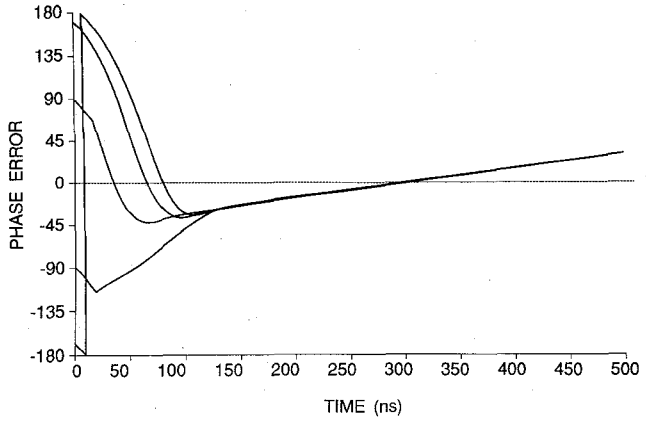

Fig. 5. Calculated EIO phase output as a function of time during the 500 ns transmitter pulse.

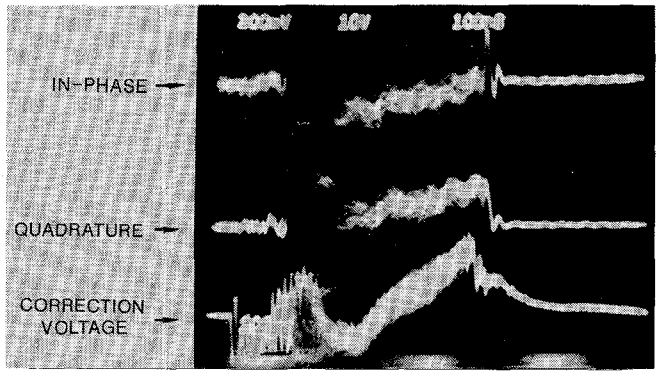

Fig. 6. Measured phase variation of the EIO output during a 500 ns pulse, 100 ns/division horizontal, 200 mV/div vertical. Both in-phase (top) and quadrature (center) outputs are shown. The bottom trace is the correction voltage applied to the EIO body during the pulse, 10 V/div.

Substituting for $d\phi(n)/dt$ from (2) gives

$$\phi(n+1) = \phi(n) + \Delta t k_e \{V_{\max} \sin[\phi(n-m)] + bt(n) + V_{os}\} \tag{4}$$

where we have taken the time delay to be $d = m\Delta t$.

Measured values of the above pertinent parameters for the 225 GHz EIO are $V_{\max} = 20$ V, $m\Delta t = 15$ ns, $b = 5 \times 10^7$ V/s, and $V_{os} = 15$ V. The parameter k_e has a value of 1.88×10^6 rad/s/V for this EIO, and the EIO tuning constant alone is 300 kHz/V. Substituting these values and initial conditions into (4) and calculating the EIO output phase by the indicated iterative technique gives the phase variation curves of Fig. 5. The four separate curves result from assuming four different initial phases for the EIO. These curves should be compared with the measured results given in Fig. 6, which shows in-phase and quadrature phase detector outputs together with the correction voltage applied to the EIO body. Note that the measured in-phase output is in good qualitative agreement with Fig. 5, with the burst of random phases at the beginning of the pulse corresponding to random initial phases for the EIO. Fig. 7 shows the free-running spectrum of the EIO, and Fig. 8 shows the spectrum of the locked source corresponding to the phase errors shown in Fig. 6. Although these results are not as good as those obtained with highly stabilized lower frequency

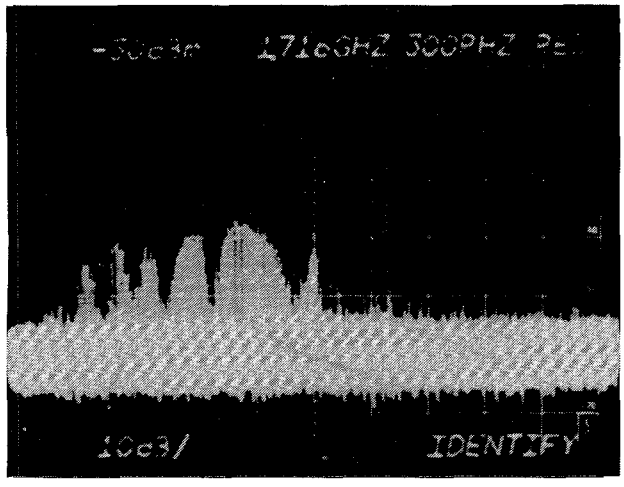

Fig. 7. Spectrum of the unlocked EIO. The frequency scale is 4 MHz/div., the vertical scale is 10 dB/div., and the resolution bandwidth is 300 kHz.

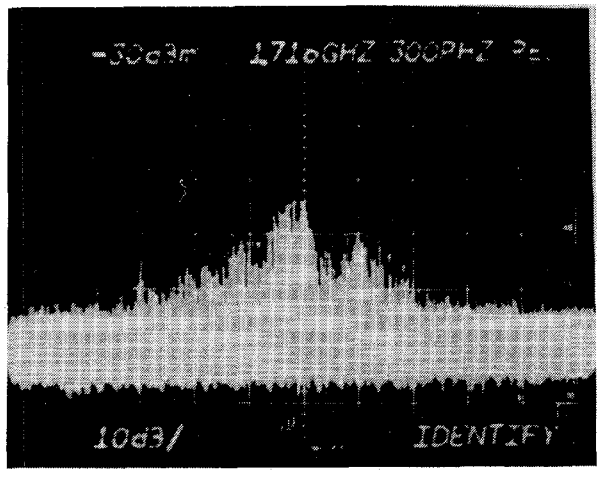

Fig. 8. Spectrum of the EIO phase locked as described herein. The parameters are the same as those of Fig. 7.

sources, they were good enough to observe Doppler returns from a variety of targets, including an armored vehicle, which showed different Doppler frequencies for body and treads, and a truck for which engine vibrations were detected.

Some comments on the degree of coherence indicated by Figs. 7 and 8 are in order. Fig. 7 is the spectrum of a signal exhibiting some frequency chirp, while Fig. 8 shows that most of this chirp has been removed by phase-locking, although some asymmetry remains, consistent with a slight linear phase change as a function of time during the pulse, as predicted by the theory developed above. Both spectra are noisy, and the source of this noise is thought to be the burst of random phases which occurs at the beginning of the pulses. Depending on the initial phase error at the initiation of the pulse, the rate of phase correction in degrees per second will vary. Each of these correction rates corresponds to a separate frequency, which causes the noise exhibited in Figs. 7 and 8, since each spectrum comprises the contributions of many pulses. This burst of random frequencies will also cause the Doppler spectra to be noisy. This is because each of them, upon reflection from the target, mixes with the local oscillator to give a different Doppler frequency, and thus raises the broad-band noise floor of the Doppler spec-

TABLE II
RECEIVER SPECIFICATIONS

Parameter	Value
Mixer Noise Figure (Single Sideband)	11.0 dB, 11.5 dB*
Receiver Path Losses (See Section VI)	0.8 dB
Horn Antenna Loss (Estimated)	1.5 dB
IF Amplifier Noise Figure (Manufacturer's Specification)	2.0 dB
Total SSB System Noise Figure	15.3 dB, 15.8 dB*

*Values corresponding to two best mixers.

trum. This phenomenon is evident in the Doppler spectra to be discussed in a later section although this noise is significantly reduced by switching out the first 100 ns of the return pulse using a high-speed IF switch.

V. RECEIVER

The $f/4$ subharmonic mixer used in the receiver has been described by Schneider *et al.* [8] and by Forsythe *et al.* [9]. In this device, signal and LO power are incident on a pair of antiparallel Schottky-barrier point-contact diodes in such a way that the fourth harmonic of the LO combines with the signal to produce the intermediate frequency. The 781 MHz IF signal is amplified as shown in the block diagram and mixed with the output of a 781 MHz cavity oscillator in both in-phase and quadrature modes to generate I and Q signals, which are further amplified by video amplifiers. These two outputs are the final system outputs, and the frequency content of the pulses is just that due to the radial velocity of the target. The I and Q signals were intended to be used in signal processing, but funding limitations precluded the development of this subsystem, so that most of the measurements made with the radar were made in A-scope mode. Table II summarizes the performance levels achieved by this receiver, including all of the loss contributions from the antenna system and duplexer.

VI. ANTENNA AND DUPLEXER

To minimize losses, the antenna and duplexer were fabricated with quasi-optical components as far as possible. The use of lossy WR-5 waveguide was minimized. Identical conical corrugated horns were used in the receiver and the transmitter for optimal matching of these two transmission paths [10], [11]. This design minimizes spillover losses and gives low side lobes and stray radiation. These horns were designed at Georgia Tech and fabricated elsewhere by an electroforming process in which an aluminum mandrel is first gold plated and then coated with electroformed copper. The mandrel is then dissolved with acid, leaving the desired precise gold-plated corrugations on the inside of the copper horn.

The lenses were machined from extruded poly-4-methylpentene-1 plastic, manufactured and marketed under the trademark name TPX by Mitsui Petrochemical Industries. The lens surfaces were machined with a hyperbolic figure to minimize spherical aberrations. The diameter of the primary lens was specified to be 152 mm (6.00 in) by the sponsor of this work. Two sets of lenses were made. One with polished surfaces was used for system alignment with a visible light source, since TPX is sufficiently transparent to visible light that it can be used for this purpose. The other set was antireflection treated by machining circular grooves in the surfaces of both lens faces to form quarter-wave matching layers [12]. It was necessary to make the grooves circular so that the lenses would pass the two orthogonal polarizations equally.

It is of interest to state why TPX was used for lens fabrication instead of the more commonly used Rexolite (a cross-linked polystyrene). Both plastics are known to be highly transparent at 95 GHz, but TPX has an advantage at higher frequencies. At the beginning of the program, before the 225 GHz source was available, a series of transmission measurements was made on Rexolite and TPX using an optically pumped far-infrared laser together with a ratioing transmission measuring system. The results of these measurements showed that TPX has an absorption coefficient of < 0.1 dB/cm at 244 GHz, while Rexolite has an absorption coefficient of 0.44 dB/cm. This advantage of TPX over Rexolite becomes more pronounced at still higher frequencies; for example at 526 GHz TPX measures 0.28 dB/cm, while measurements on Rexolite give 1.50 dB/cm. These results are in good agreement with published measurements [13] on these two materials.

The quarter-wave plate was fabricated from sapphire, which has a large intrinsic birefringence ($n_e - n_o = 0.345$). This value was derived from measured polarization ellipticity at 247 GHz using an optically pumped far-infrared laser and grid polarization analyzer. This value also agrees well with values of the optical constants of sapphire extrapolated from published results obtained above 600 GHz [13]–[16]. In order to act as a quarter-wave plate, a sapphire crystal must be cut with its c axis parallel to the plate faces, and it must be oriented so that the E vector of the input radiation bisects the fast and slow axes, which are oriented at 90° relative to each other. The sapphire crystal was fabricated to be 177.8 mm in diameter and 4.89 mm thick. At this thickness, it is a fifth-order quarter-wave plate. Tests of this optical element showed that the ratio of orthogonal to input polarization of radiation from the transmitter EIO at 225 GHz, after making two transits through the plate, was 20 dB.

Since sapphire has an average index of refraction of 3.24, it must be antireflection coated; otherwise the reflection losses will be about 30% per surface. Based on the authors' familiarity with plastic materials, it was decided that Mylar, with a refractive index of 1.7, which is close to the square root of the average sapphire index, would be a good candidate for this application. The optimum film thickness for this matching layer is $\lambda/4n = 195$ μm, and the nearest commercially available thickness to this value is 178 μm. For good performance as a matching layer, it is necessary that the Mylar be in good contact with the sapphire, and this requirement was met by building a vacuum fixture by which the two materials could be pulled together. After fabrication, the reflection losses in the sapphire/Mylar interface were determined to be -0.06 dB, with the side away from the transmitter (second surface) yielding -0.03 dB. This level of reflectivity gives a stray signal into the receiver 22 dB below the transmitter radar output, which is apparently not enough to damage the mixer diodes.

The polarizing beam splitter is an aluminum wire grid on Mylar. The conductors were chosen to be 5 μm wide and the period was 10 μm. The grids were printed through a mask which was in vacuum contact with the photoresist and alu-

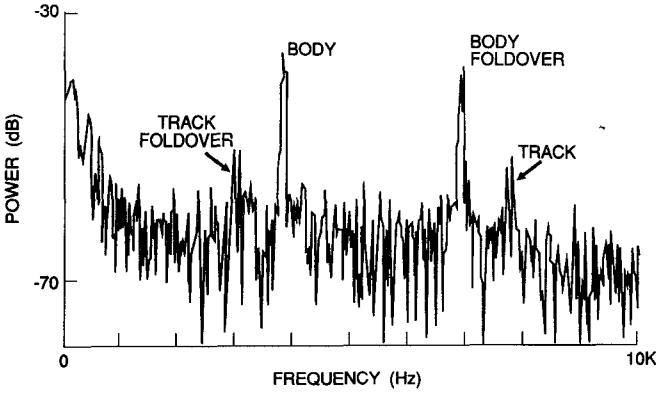

Fig. 9. Doppler spectrum of a tracked vehicle target moving radially at 2.6 m/s. Contributions from the body, treads, and fold over due to these lines are evident in the trace.

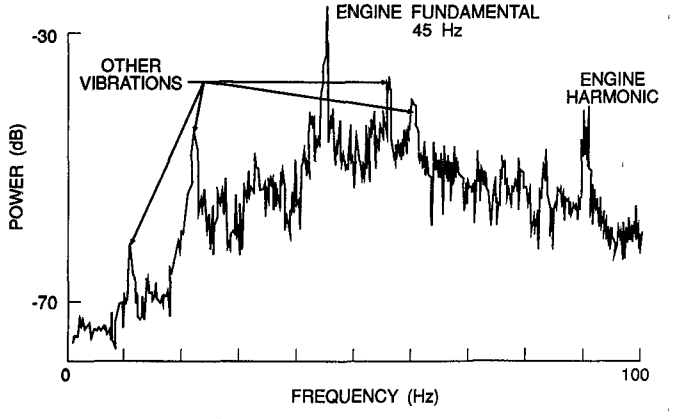

Fig. 10. Doppler spectrum of a stationary truck with its engine running at 2700 r/min. The other Doppler spectral lines are due to engine harmonics and other body vibrations.

minum-coated Mylar substrate. Performance measurements made on these components showed that they had a reflectivity ratio of 20 dB with the grid wires parallel to the plane of input polarization and a transmission loss of 0.02 dB with the wires perpendicular to the input polarization. It is presumed that the power reflected in this latter mode goes into the receiver, but note that its polarization is orthogonal to that to which the receiver is sensitive, so that it does not add to the unwanted radiation incident on the mixer.

VII. Results

The most significant results obtained with this radar are the Doppler measurements made on tracked vehicles and trucks. Fig. 9 shows the Doppler spectrum of a tracked vehicle moving at a velocity of 2.6 m/s. There is a major contribution to the Doppler spectrum at 3.9 kHz corresponding to the body and another line at 7.8 kHz due to the tracks. Body and track foldover spectra, resulting from the Doppler frequencies combining with the second harmonic of the 12 kHz radar PRF, are also shown. The Doppler spectrum of a stationary truck at a range of 900 m is shown in Fig. 10. The truck engine was running at 2700 r/min, corresponding to the 45 Hz Doppler return. The other lines are due to harmonics and subharmonics of this frequency and to other vibrations occurring in the truck body.

The observation of Doppler returns is not necessarily an indication of radar coherence, since such returns might be

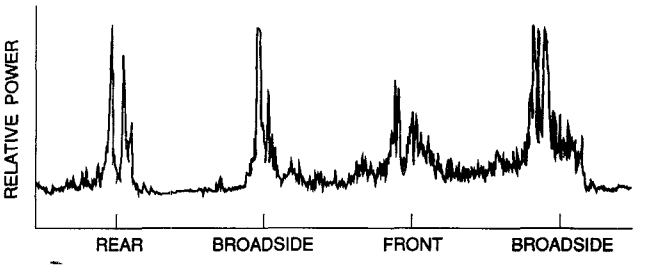

Fig. 11. Return from a $2\frac{1}{2}$ ton truck driven in a circle at a range of 900 m.

generated by beating of reflections from a moving target with those from stationary clutter within the same range cell. The radar described in this paper is vulnerable to this problem, since the 500 ns pulse width implies a range cell 75 m in extent, so that stationary clutter 37.5 m on either side of the target might give rise to such false Doppler returns. Although measurements of clutter returns with no target present were not made to verify that there were no significant scatterers within the target range cell, we believe, based on visual observation of the terrain on which the experiments were conducted, that no clutter existed which would cause such false Doppler phenomena. We therefore conclude that the results presented in this paper are an indication of radar coherence, subject to the limitations discussed in Section IV. An even more compelling reason for concluding that the radar is coherent is that all Doppler returns disappear when the phase lock is turned off.

In addition to the Doppler results discussed above, some additional results were obtained with the radar operated in an A-scope mode. To obtain these results, a matched filter with a band-pass of 2 MHz corresponding to the 500 ns radar pulse width was used. Returns from unknown targets at ranges up to 3.5 km were obtained with good signal-to-noise ratio. Because the optical duplexer was used instead of a transmit–receive switch, it was found that the radar has a very short minimum range. Although a saturation region caused by the transmitter pulse is evident in A-scope returns, it simply represents a region of reduced sensitivity, and targets within this region are still visible because they generally have large returns. It was possible using this radar to observe Doppler spectra at ranges less than 100 m.

Some results at varying target aspects were also obtained. Fig. 11 is a record of the relative return from a $2\frac{1}{2}$ ton truck driven in a circle at a range of 900 m. For all of the measurements described in this section, the weather was excellent; in poor weather one might expect that the radar operational range would be shorter.

VIII. Conclusions

We have shown that it is possible to build a pulsed radar operating in the 230 GHz atmospheric window which is capable of observing Doppler returns. The degree of coherence implied by these measurement is not quantitatively determined, but measurements of the transmitter phase indicate improvement owing to phase locking and qualitative agreement with theory. These reservations are expressed because noncoherent radars may exhibit coherence effects without any means of phase control, as discussed in Section VII.

Although all of the technologies represented in this system were well developed at the time it was assembled and tested, we believe that the combination of approaches used in this radar is unique, not only to the 230 GHz band, but to any radar operating at any frequency. The hard-tube modulator was designed by Georgia Tech originally for this system, and has been used on all cathode-modulated EIO-based radars built at Georgia Tech since its inception. The phase-locking approach was used at Georgia Tech to lock a pulsed orotron oscillator [17], but other specific instances of the use of this pulsed locking method are not known, although there is some indication that it may have been used for locking pulsed magnetrons several years ago. The $f/4$ subharmonic mixer used in this receiver allows the use of a fundamental, reliable Gunn LO source and is an extension of the $f/2$ subharmonic mixer work done by Schneider *et al.* [8] and by Forsythe *et al.* [9]. The optical polarization duplexer has been used for several years in laser radars [18], and is logically extended to the 230 GHz band because of the availability of appropriate materials, such as large single crystals of sapphire and plastics designed for other applications. The method of matching or antireflection coating surfaces described in this paper has of course been used for many years, but the techniques devised and the results obtained are of interest to other workers in the MMW and far-infrared fields.

The results of this paper show that the well-known concepts and techniques applicable to radars built at lower frequencies may also be used for radars operating at least to 225 GHz. While it is evident that results obtained at 225 GHz are not as good as those at lower frequencies, the development of suitable components over the next few years will provide the means for further exploitation of this potentially useful band of frequencies.

Acknowledgment

The authors appreciate the contributions of V. T. Brady, D. S. Ladd, A. McSweeney, J. M. Newton, O. A. Simpson, and M. J. Sinclair to this work. Discussions with G. W. Ewell of Georgia Tech on radar source coherence are gratefully acknowledged.

References

[1] H. J. Liebe and D. H. Layton, "Millimeter-wave properties of the atmosphere: Laboratory studies and propagation modeling," NTIA Rep. 87-224, National Telecommunications and Information Administration, Boulder, CO, Oct. 1987.

[2] R. E. McIntosh, R. M. Narayanan, J. B. Mead, and D. H. Schaubert, "Design and performance of a 215 GHz pulsed radar system," *IEEE Trans. Microwave Theory Tech.*, vol. 36, pp. 994–1001, June 1988.

[3] R. E. McIntosh and J. B. Mead, "Polarimetric radar scans terrains for 225-GHz images," *Microwaves and RF*, p. 91, Oct. 1989.

[4] R. M. Narayanan, C. C. Borel, and R. E. McIntosh, "Radar backscatter characteristics of trees at 215 GHz," *IEEE Trans. Geosci. Remote Sensing*, vol. 26, pp. 217–228, May 1988.

[5] R. L. Hartman and P. W. Kruse, "Quasi-imaging near millimeter radar," presented at Fourth Int. Conf. Infrared and Millimeter Waves, Miami Beach, FL, Dec. 10–15, 1979.

[6] *Introduction to Extended Interaction Oscillators*, Data Sheet 3445 5M 11/75, Varian Associates of Canada, Ltd., Georgetown, Ont., Canada, 1975.

[7] G. M. Conrad and J. C. Butterworth, "Extended interaction oscillator/amplifier modulator technology," presented at Eighth Int. Conf. Infrared and Millimeter Waves, Miami Beach FL, Dec. 12–17, 1983.

[8] T. F. McMaster, M. V. Schneider, and W. W. Snell, "Millimeter-wave downconverter with subharmonic pump," in *IEEE MTT-S Int. Microwave Symp. Dig.* (Cherry Hill, NJ), 1976.

[9] R. E. Forsythe, V. T. Brady, and G. T. Wrixon, "Development of a 183 GHz subharmonic mixer," presented at IEEE MTT-S Int. Microwave Symp., Orlando, FL, May 1978.

[10] M. S. Narasimhan, "Corrugated conical horn as a space feed for phased-array illumination," *IEEE Trans. Antennas Propagat.*, vol. AP-22, pp. 720–722, Sept. 1974.

[11] B. M. Thomas, "Design of corrugated conical horns," *IEEE Trans. Antennas Propagat.*, vol. AP-26, pp. 367–372, 1978.

[12] T. Morita and S. B. Cohn, "Microwave lens matching by simulated quarter-wave transformers," *IRE Trans. Antennas Propagat.*, p. 33, Jan. 1956.

[13] J. R. Birch, J. D. Dromey, and J. Lesurf, "The optical constants of some low-loss polymers between 4 and 40 cm^{-1}," National Physical Laboratory (United Kingdom) Rep. DES 69, Feb. 1981.

[14] E. E. Russell and E. E. Bell, "Optical constants of sapphire in the far infrared," *J. Opt. Soc. Amer.*, vol. 57, pp. 543–544, 1967.

[15] E. V. Lowenstein, D. R. Smith, and R. L. Morgan, "Optical constants of far infrared materials 2: Crystalline solids," *Appl. Opt.*, vol. 12, pp. 398–405, 1973.

[16] S. Roberts and D. D. Coon, "Far infrared properties of quartz and sapphire," *J. Opt. Soc. Amer.*, vol. 57, pp. 1023–1029, 1962.

[17] R. W. McMillan *et al.*, "Results of phase and injection locking of an orotron oscillator," *IEEE Trans. Microwave Theory Tech.*, vol. 37, pp. 1828–1830, Nov., 1989.

[18] M. J. Post, "Atmospheric infrared backscattering profiles: Interpretation of statistical and temporal properties," NOAA Tech. Memorandum ERL WPL-122, National Oceanic and Atmospheric Administration, Boulder, CO, May 1985.

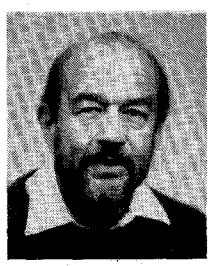

Robert W. McMillan (M'82–SM'83) was born in Sylacauga, AL. He was educated at Auburn University, Rollins College, and the University of Florida.

He has been at the Georgia Tech Research Institute since 1976 and has worked primarily in the area of millimeter-wave technology. Prior to joining GTRI, he worked at Martin Marietta Aerospace in Orlando, FL, and at Westinghouse Electric Corporation in Baltimore, MD.

Dr. McMillan is a member of the Optical Society of America.

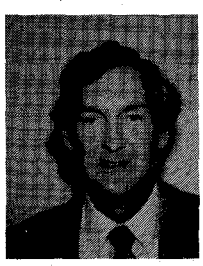

C. Ward Trussell, Jr., received the B.S. degree in physics from Clemson University in 1965 and the Ph.D. degree in physics from the University of Virginia in 1969.

Since 1969, he has been with the U.S. Army's Center for Night Vision and Electro-Optics at Ft. Belvoir, VA. He is currently a team leader in the Laser Division developing solid-state laser technology. His major projects at C2NVEO have included semiconductor lasers, image intensifiers, millimeter-wave technology, and solid-state lasers.

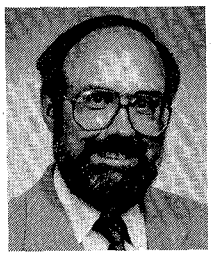

Ronald A. Bohlander was born in Omaha, NB. He received the B.S. degree in astronomy from Case Western Reserve University, Cleveland, OH, in 1968, the M.S. degree in physics from the University of Colorado, Boulder, in 1972, and the Ph.D. degree in physics from the Imperial College of Science and Technology, London University, London, England, in 1979.

He was a Research Physicist in the University of Colorado Physics Department from 1971 to 1973, where he investigated millimeter-wave atmospheric transmission and air pollution gas analysis techniques. He subsequently went to the Appleton Laboratory in England, where he conducted spectroscopic researches on water vapor covering ultraviolet to millimeter wavelengths. In 1979, he joined the Georgia Tech Research Institute in Atlanta, where he has investigated optical design in millimeter-wave systems and atmospheric effects on millimeter-wave propagation. He currently leads research in advanced sensors and information systems for industrial automation and heads the Manufacturing Technology Program Office in GTRI.

Dr. Bohlander is a member of Tau Beta Pi and the Society of Manufacturing Engineers.

✠

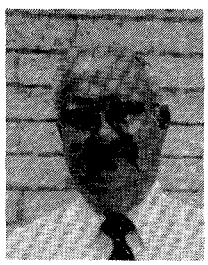

J. Clark Butterworth received an associate in science degree in electronics and radio from the Southern Technical Institute, Marietta, GA, in 1951.

He then joined Georgia Tech's Engineering Experiment Station (now Georgia Tech Research Institute). After completing military service in the U.S. Army from 1954 to 1956, he rejoined the Georgia Institute of Technology, where he remained until retiring in 1987 as Branch Head of the Radar Technology Branch of the Institute's Radar and Instrumentation Laboratory.

Mr. Butterworth authored or coauthored some 29 technical reports and journal articles during the years 1960 to 1987. After retirement he became Principal Engineer for Electo Systems International (1987–1988). He is now with Pulse Technology Inc., Kennesaw, GA.

✠

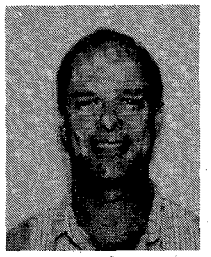

Ronald E. Forsythe was born in Tucson, AZ, on September 24, 1952. He received the B.S.E. degree and the M.S.E. degree from the University of South Florida, Tampa, in 1978 and continued his studies for the Ph.D. degree at Georgia Tech, specializing in EM theory.

He worked at the Georgia Tech Research Institute from 1976 to 1986, during which time he progressed from student assistant to Senior Research Engineer and MM Wave Device Branch Leader. He specialized in mm-wave devices and subsystem design and development in the areas of radiometry, radar, and EW systems. These include the development of ultraminiature low-noise broad-band down-converters, subharmonically pumped mixers, multiband scanning radiometers, and direction finding receivers. These developments covered the entire 30 to 300 GHz mm-wave frequency range. He left GTRI in 1986 to eventually become Vice President of Engineering at Millimeter Wave Technology, during which time he developed mm-wave radars, frequency agile 60 GHz communication systems, remote ice detection systems, portable relectometers for measuring RAM performance, radar target simulation systems (both microwave and mm-wave), and radar absorbing fabrics. He left Millimeter Wave Technology in June 1989 and is currently self-employed doing component and subsystem development as Forsythe Techonologies. His current activities are in the areas of mm-wave seeker design and development, ultralinear mm-wave FMCW radars, mm-wave target simulators, multiband RF converters, and up/down-converter development.

Mr. Forsythe is a member of Tau Beta Pi and Phi Kappa Phi. He has participated in numerous IEEE paper presentations and has been a local chapter speaker on the topic of subharmonically pumped mm-wave mixers. He has also participated as a lecturer at the mm-wave short course given at Georgia Tech.